CHINESE OPTICS LETTERS

Vol. 19, No. 9 | September 2021

GSA and ESA dual-wavelength pumped 2.3 μm Tm:YLF laser on the $^3H_4 \rightarrow {}^3H_5$ transition

Fei Wang (王 飞), Haitao Huang (黄海涛)*, Haiwei Chen (陈海伟), Yushuo Bao (鲍玉朔), Zihan Li (李子涵), and Deyuan Shen (沈德元)

School of Physics and Electronic Engineering, Jiangsu Normal University, Xuzhou 221116, China

*Corresponding author: hht840211@163.com

Received January 15, 2021 | Accepted March 3, 2021 | Posted Online May 31, 2021

The population trapping effect of the $^3F_4$ level is an important factor limiting the power scaling of the 2.3 μm thulium (Tm) laser on the $^3H_4 \rightarrow {}^3H_5$ transition. In this Letter, we demonstrate a novel scheme of ground state absorption (GSA) ($^3H_6 \rightarrow {}^3H_4$) and excited state absorption (ESA) ($^3F_4 \rightarrow {}^3H_4$) dual-wavelength pumped 2.3 μm Tm lasers. Introducing an ESA pumping process can accurately excite the Tm^{3+} ions accumulated in the $^3F_4$ level to the $^3H_4$ level, constructing a double populating mechanism for the upper laser level $^3H_4$. A proof-of-principle experimental demonstration of the GSA (785 nm) and ESA (1470 nm) dual-wavelength pumped 2.3 μm Tm:$LiYF_4$ (Tm:YLF) laser was realized. A maximum continuous-wave output power of 1.84 W at 2308 nm was achieved under 785 and 1470 nm dual-wavelength pumping, increased by 60% compared with the case of 785 nm single-wavelength pumping under the same resonator condition. Our work provides an efficient way to achieve higher output power from 2.3 μm Tm-doped lasers on the $^3H_4 \rightarrow {}^3H_5$ transition.

Keywords: 2.3 μm thulium laser; $^3H_4 \rightarrow {}^3H_5$ transition; dual-wavelength pumping.

DOI: 10.3788/COL202119.091405

1. Introduction

In recent years, 2.3 μm laser operation of thulium (Tm)-doped materials on the $^3H_4 \rightarrow {}^3H_5$ transition has attracted increasing attention[1-5]. From the perspective of laser generation, Tm^{3+} ions have strong ground state absorption (GSA) of $^3H_6 \rightarrow {}^3H_4$ at ~0.8 μm, matching well with the emitting wavelength of commercial AlGaAs laser diodes (LDs)[6–11]. The lower energy level $^3H_5$ is at the position of ~9000 cm^{-1} above the ground state $^3H_6$, which can support four-level laser operation at room temperature. Furthermore, it is easy to obtain high-quality laser materials compared with the Cr^{2+}-doped lasers. From the perspective of laser application, 2.3 μm lasers can find potential application in noninvasive medical diagnosis and important gas detection due to the weak absorption of water and strong absorption of N_2O, CO, and CH_4 in the 2.3 μm region[12–16].

Conventional pumping at ~0.8 μm and upconversion pumping at ~1 μm have been developed to achieve laser oscillation of Tm-doped materials on the $^3H_4 \rightarrow {}^3H_5$ transition[17–20]. Under conventional pumping at ~0.8 μm, Tm^{3+} ions can be directly excited from the ground level $^3H_6$ to the $^3H_4$ level. However, the metastable $^3F_4$ level is also populated by a cross relaxation (CR) process of $^3H_6 + {}^3H_4 \rightarrow {}^3F_4 + {}^3H_4$, yielding two excited ions at the $^3F_4$ level for each absorbed pump photon[21,22]. The CR process is a favorable factor for the $^3F_4 \rightarrow {}^3H_6$ transition at 1.9 μm, but it is very unfavorable for 2.3 μm laser generation. On the one hand, the increase of population at the $^3F_4$ level directly corresponds to the decrease of Tm^{3+} ions at the $^3H_4$ level. On the other hand, the accumulation of Tm^{3+} ions at the $^3F_4$ level will further aggravate the related energy transfer losses. Therefore, the CR process plays a negative role for the 2.3 μm laser transition in this conventional pumping scheme. Recently, we reported simultaneous dual-wavelength laser operation at 1.9 and 2.3 μm in Tm:$LiYF_4$ (Tm:YLF) pumped by a 785 nm LD. It was found that the output powers for the $^3F_4 \rightarrow {}^3H_6$ and $^3H_4 \rightarrow {}^3H_5$ transitions were both linearly increased with the 785 nm LD pump power, showing that a considerable population in the $^3F_4$ level exists[8].

In the upconversion pumping scheme, the population of the $^3H_4$ level was achieved by a resonant excited state absorption (ESA) process of $^3F_4 \rightarrow {}^3F_{2,3}$ or $^3F_4 \rightarrow {}^3H_4$, with the $^3F_4$ level populated early by a matched GSA process of $^3H_6 \rightarrow {}^3H_5$ or $^3H_6 \rightarrow {}^3F_4$. At 1040, 1055, and 1451 nm, 2.3 μm laser operation of 3.5% (atomic fraction) Tm:YLF upconversion pumped has been demonstrated[18]. The CR process plays a positive role to enhance the probability of ESA. Limited by the fact that the single upconversion pumping wavelength should be located in the cross region of the GSA and ESA spectra, the

phonon-assisted weak GSA at ~1 μm and 1.45 μm in Tm:YLF cannot provide more Tm^{3+} ions for the ESA process starting from the $^3F_4$ level.

In this Letter, we propose a novel dual-wavelength pumping scheme for the 2.3 μm Tm lasers. As shown in Fig. 1, the GSA of $^3H_6 \rightarrow {}^3H_4$ at ~0.8 μm and ESA of $^3F_4 \rightarrow {}^3H_4$ at ~1.45 μm for Tm:YLF were jointly used to build a double populating mechanism for the upper laser level $^3H_4$. The first step is to realize the population of the $^3H_4$ level induced by the strong resonant GSA ($^3H_6 \rightarrow {}^3H_4$) by 0.8 μm pumping. Meanwhile, the CR process will further populate the metastable $^3F_4$ level. In the second step, a second 1.45 μm pump light can be introduced, and the Tm^{3+} ions accumulated at the $^3F_4$ level are further precisely excited to the $^3H_4$ level by a strong ESA process of $^3F_4 \rightarrow {}^3H_4$. In contrast with the conventional single-wavelength pumping at ~0.8 μm, the CR process serves as a positive factor in dual-wavelength pumping due to the introduction of ESA. Compared with the single-wavelength upconversion pumping scheme, there is no need to balance GSA and ESA in the dual-wavelength pumped 2.3 μm Tm laser. The two pumping wavelengths used can be selected independently to maximize GSA and ESA, respectively. The excited Tm^{3+} ions at the $^3F_4$ level required for the ESA process can be effectively supplemented by the strong CR process pumped at ~0.8 μm.

Recently, the cascaded dual-wavelength pumping scheme has been demonstrated in Er-doped lasers to achieve mid-infrared output at 3.5 μm[23]. In the cascaded pumping scheme, one pumping wavelength was used to pump Er^{3+} ions populated in the ground state ($^4I_{15/2}$) to a long-lived intermediate excited state ($^4I_{11/2}$). Then, a second ESA pumping wavelength can pump the Er^{3+} ions from the intermediate state to the upper laser level ($^4F_{9/2}$) for the construction of the laser transition of $^4F_{9/2} \rightarrow {}^4I_{9/2}$. Compared with the cascade pumping scheme, the proposed GSA and ESA dual-wavelength pumping for the Tm-doped lasers on $^3H_4 \rightarrow {}^3H_5$ has two significant differences. From the population mechanism for the upper level of target laser transition, the $^3H_4$ level can be populated by the GSA and ESA process. From the population mechanism for the intermediate excited state, the remarkable CR process in Tm^{3+} ions can provide more active ions for the ESA process. In the cascaded pumping scheme, the first pumping wavelength is just for establishing a population of active ions in the intermediate excited state. The power at the first pumping wavelength is required at a relatively low level to replenish ions that spontaneously decay to the ground state.

A proof-of-principle experimental demonstration of a GSA (785 nm) and ESA (1470 nm) dual-wavelength pumped 2.3 μm Tm:YLF laser was realized. Under 785 nm single-wavelength pumping, the maximum continuous-wave (CW) output powers of 1.5%-doped Tm:YLF crystal were 1.15 W and 584 mW for 1.5% and 2.8% output couplers (OCs), respectively. When the second pump beam of 1470 nm was introduced, the oscillation thresholds of the 2.3 μm laser were reduced by 66.7% and 55.6%, and the maximum CW output powers were increased to 1.84 W and 1.2 W for 1.5% and 2.8% OCs, respectively. This shows that the introduction of the ESA pumping process of the $^3F_4 \rightarrow {}^3H_4$ transition is beneficial to further increase the Tm^{3+} ions population of the $^3H_4$ level, constructing a double populating mechanism for the upper laser level $^3H_4$ of a 2.3 μm transition. Our work shows that the GSA ($^3H_6 \rightarrow {}^3H_4$) and ESA ($^3F_4 \rightarrow {}^3H_4$) dual-wavelength pumping scheme is an effective method to generate higher output power from 2.3 μm Tm lasers.

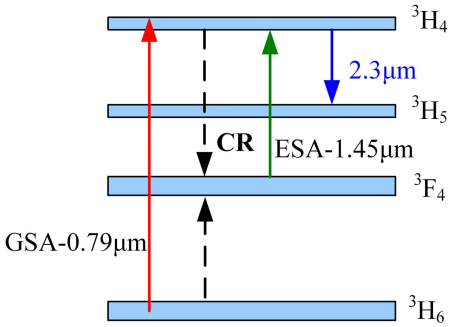

Fig. 1. Schematic diagram for GSA and ESA dual-wavelength-pumped 2.3 μm thulium laser. GSA, ground state absorption; ESA, excited state absorption; CR, cross relaxation.

2. Experimental Setup

The experimental arrangement of the GSA and ESA dual-wavelength pumped 2.3 μm Tm:YLF laser is shown in Fig. 2. As shown in Ref. [18], strong GSA ($^3H_6 \rightarrow {}^3H_4$) absorption was observed between 780 and 800 nm. The most intense ESA absorption for the $^3F_4 \rightarrow {}^3H_4$ transition occurs at 1452 nm with an FWHM of 3.7 nm for Tm:YLF. Then, two LD pump sources were used. The first one was a 785 nm AlGaAs LD, with the wavelength matching the strong GSA process ($^3H_6 \rightarrow {}^3H_4$) with an absorption cross section of $\sim 7 \times 10^{-21}$ cm^2 at 785 nm[18]. The output-coupling fiber of the 785 nm LD had a core diameter of 400 μm and a numerical aperture of 0.22. The second one was a 1470 nm LD corresponding to the ESA process ($^3F_4 \rightarrow {}^3H_4$), whose output-coupling fiber had a core diameter of 200 μm and a numerical aperture of 0.11. Limited by the available experimental conditions, the central wavelength of the second LD used deviates from the strongest ESA absorption peak of 1452 nm. But, 1470 nm also overlapped the sideband of the

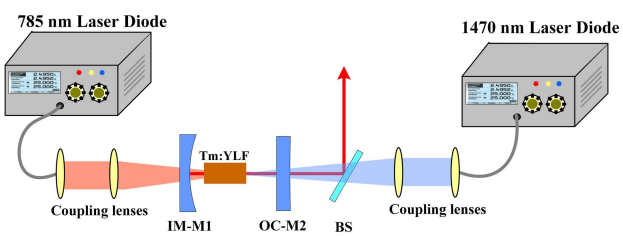

Fig. 2. Experimental arrangement for the GSA and ESA dual-wavelength LD-pumped Tm:YLF laser. IM, input mirror; OC, output coupler; BS, beam splitter.

$^3F_4 \rightarrow {}^3H_4$ ESA transition with an absorption cross section of $\sim 1.4 \times 10^{-21}$ cm^2[18]. The two-mirror laser cavity was composed of an input mirror (IM) and an OC. The IM was a plane-concave mirror with a curvature radius of 300 mm, which was designed to be high-reflection coated at 2250–2500 nm ($R > 99.8\%$) and high-transmittance coated at 785 nm. Two kinds of plano-plane OCs were used to evaluate the laser output characteristics. OC1 and OC2, respectively, had a transmittance of 1.5% and 2.8% across the region of 2250–2400 nm. The suppression of 1.9 μm oscillation ($^3F_4 \rightarrow {}^3H_6$) was achieved by increasing the transmittance of the output mirror at this waveband. The transmittances of OC1 and OC2 at 1.9 μm were measured to be 90%. Because there is no suitable combiner for the dual-wavelength pump light, the two pumping beams were, respectively, coupled into the laser crystal from the left and right sides of the laser cavity, establishing the double-end pumping configuration. The 1:1 and 2:1 coupling focusing systems were used to reshape the 785 nm pump beams, generating the pump spots with the diameters of 400 and 200 μm, respectively. For the 1470 nm pump light, the diameter of the spot inside Tm:YLF can be chosen between 200 and 400 μm, respectively, by the 1:1 and 1:2 coupling focusing systems. A beam splitter (BS) coated with high transmittance at 1.45 μm and high reflection at 2.3 μm was used to separate the pump and laser beams. An *a*-cut 4 mm × 4 mm × 8 mm Tm:YLF crystal with 1.5% doping concentration was used. The two 4 m × 4 m light-passing faces of the crystal were anti-reflection coated at 780–810 nm and 2280–2350 nm. The laser crystal was wrapped with indium foil and mounted in a copper block cooled by water at a temperature of 15°C.

3. Experimental Results and Discussions

The laser output performance under single-wavelength 785 nm pumping for different OCs was first studied. The used 785 nm pump spot in Tm:YLF is 400 μm in diameter. The laser spectrum was measured using a spectrometer (Yokogawa AQ6375), as shown in Fig. 3, with a central wavelength of 2308 nm observed for the two OCs. The output powers with regard to incident

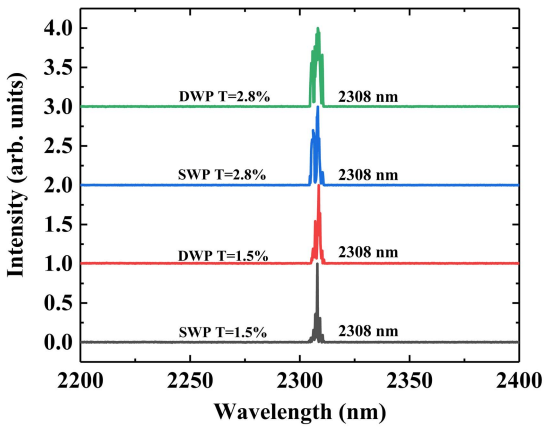

Fig. 3. Typical laser emission spectra measured at maximum output power. SWP, single-wavelength pumping; DWP, dual-wavelength pumping.

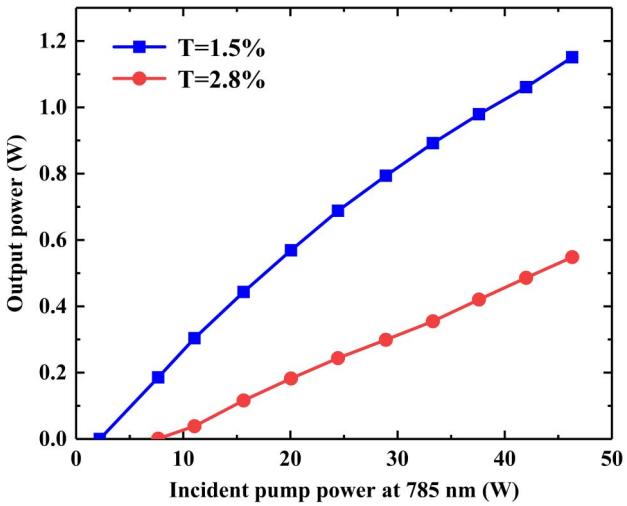

Fig. 4. Output powers of 2.3 μm laser versus the incident 785 nm pump powers.

pump powers were shown in Fig. 4. Using OC1 ($T = 1.5\%$), the maximum CW output power of 1.15 W was obtained, and the slope efficiency was 2.6% with regard to the incident pump power. The absorbed pump power of Tm:YLF under laser conditions was further measured, resulting in a slope efficiency of 19% with regard to absorbed pump power for OC1. As for OC2 ($T = 2.8\%$), the laser generated a maximum output power of 584 mW. The corresponding slope efficiency was 1.5% and 12.3% relative to the incident pump power and absorbed pump power, respectively. The saturation of output power was not observed with the increase of pump power for the two OCs. It was experimentally found that the 2.3 μm Tm-doped laser performance on the $^3H_4 \rightarrow {}^3H_5$ transition was sensitive to the resonator loss. Multiphonon decay and Tm^{3+} ion-pair CR can nonradiatively depopulate the $^3H_4$ upper laser level, resulting in reduced fluorescence lifetime and correspondingly high lasing threshold. Therefore, low output transmittance was more conducive to efficient laser operation, as demonstrated in Ref. [24].

Then, the second pump beam of 1470 nm with a diameter of 200 μm was injected to the Tm:YLF, constructing the GSA and ESA dual-wavelength pumping scheme. To characterize the effect of the ESA pumping process on the 2.3 μm laser transition, the dependence of 2.3 μm laser output powers on the incident 1470 nm pump powers under different given incident 785 nm pump powers was first studied, with the results shown in Figs. 5(a) and 5(b). Obviously, the introduction of 1470 nm pump light leads to a significant increase of 2.3 μm output power. This successfully demonstrates the effectiveness of the ESA pumping process in increasing the population at the $^3H_4$ level. It should be noted that 2.3 μm laser output was not achieved under the 1470 nm single-wavelength pumping. On the whole, 1.8 W CW output power at 2308 nm was obtained for OC1 ($T = 1.5\%$) under dual-wavelength pumping. The output power is increased by 57% compared with 785 nm single-wavelength pumping. For OC2 ($T = 2.8\%$), a maximum CW laser output of 1.2 W at 2308 nm was obtained, which increased

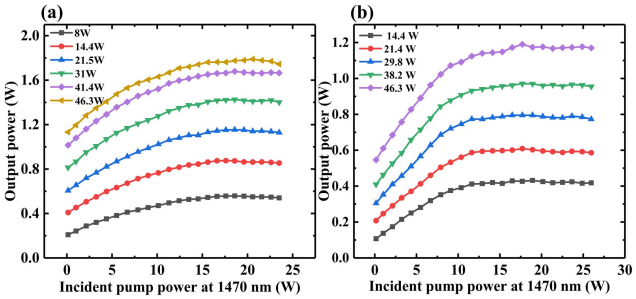

Fig. 5. Output powers of 2.3 μm laser versus incident 1470 nm pump powers under different given incident 785 nm pump powers. (a) $T = 1.5\%$ OC; (b) $T = 2.8\%$ OC.

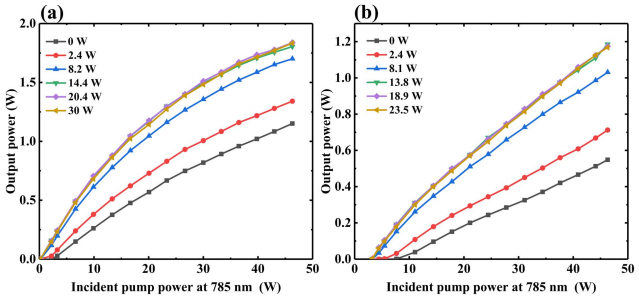

Fig. 6. Output powers of 2.3 μm laser versus incident 785 nm pump power under different given incident 1470 nm pump powers. (a) $T = 1.5\%$ OC; (b) $T = 2.8\%$ OC.

by 104% with regard to the case of 785 nm pumping. Due to the use of the double-end pumping configuration, the absorbed 785 and 1470 nm pump power cannot be measured. So, the incident pump power was used in the related discussions.

It can be seen from Fig. 5 that the variations of 2.3 μm laser output powers with 1470 nm incident pump power can be divided into two stages: the rapid growth stage and stable stage. In the first stage, with the increased 1470 nm pump power, the Tm^{3+} ions accumulated in the $^3F_4$ level were excited to the $^3H_4$ level, then the output power of the 2.3 μm laser was increased rapidly due to the population refilling of the $^3H_4$ level. As the Tm^{3+} ions at the $^3F_4$ level were gradually consumed, the rate of increase of 2.3 μm laser output powers gradually slowed down, thus entering the stable stage. At this stage, the 2.3 μm output powers were no longer sensitive to the 1470 nm pump power, and the 2.3 μm output power remained basically unchanged in a large range of pump power. This illustrated that the Tm^{3+} ions in the $^3F_4$ level had been depleted, and the ESA process had no contribution to the population refilling of the $^3H_4$ level. Further increase of 1470 nm pump power will lead to a slight decrease of 2.3 μm laser output power. The heat accumulated in the Tm:YLF crystal should be the reason for the slight decrease of 2.3 μm laser output power. Furthermore, the ESA pump saturation power (1470 nm) can be introduced, which can be defined as the 1470 nm pump power at the point where the 2.3 μm laser output power begins to enter the stable stage under a given 785 nm pump power. With the increase of 785 nm pump power, higher-power 1470 nm pump light was required to excite more Tm^{3+} ions to the $^3H_4$ level, and the corresponding ESA pump saturation power was increased. For $T = 1.5\%$ OC1, the 1470 nm saturation power was increased from 18.1 W to 20.6 W. For $T = 2.8\%$ OC2, the 1470 nm saturation power was increased from 15.9 W to 17.4 W.

Figure 6 shows the dependence of 2.3 μm laser output powers on the incident 785 nm pump powers under different given 1470 nm pump powers. It can be seen that the introduction of the ESA pump process does not change the trend of output power increasing monotonically with 785 nm pump power (similar to the curves shown in Fig. 4). When the 1470 nm ESA pump light was introduced, the 2.3 μm laser oscillation thresholds for the $T = 1.5\%$ and $T = 2.8\%$ OCs were decreased from 3.3 W to 1.1 W and 9.9 W to 4.4 W, respectively. Using OC1 ($T = 1.5\%$), the maximum CW output power reached 1.84 W at 2308 nm. The output power was increased by 60% with regard to the case of 785 nm single-wavelength pumping under the same resonator condition. For OC2 ($T = 2.8\%$), 1.19 W CW output power at 2308 nm was obtained, with the output power doubled in comparison with the case using 785 nm pumping. It could be seen from Fig. 6 that when the 1470 nm incident pump power was less than 18.9 W and 13.3 W for OC1 and OC2, respectively, the 2.3 μm laser output powers were linearly increased with the 1470 nm pump power. When the 1470 nm pump power was greater than 18.9 W and 13.3 W, the increase of 1470 nm pump power did not contribute significantly to the increase of 2.3 μm output power.

Figure 7 shows the 2.3 μm laser output power under GSA and ESA dual-wavelength pumping for different combinations of 785 and 1470 nm pump spots with OC1 ($T = 1.5\%$). Four kinds of spot combinations (400 μm:200 μm, 400 μm:400 μm, 200 μm:400 μm, and 200 μm:200 μm) were exploited, corresponding to the diameter of spot from 785 nm to 1470 nm. The achieved maximum output powers were 1.84 W, 1.52 W, 0.92 W, and 1.05 W, respectively. The corresponding output

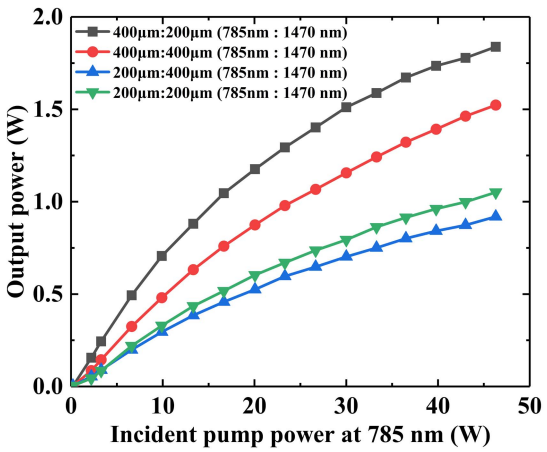

Fig. 7. Output powers of 2.3 μm laser under GSA and ESA dual-wavelength pumping for different combinations of 785 and 1470 nm pump spots.

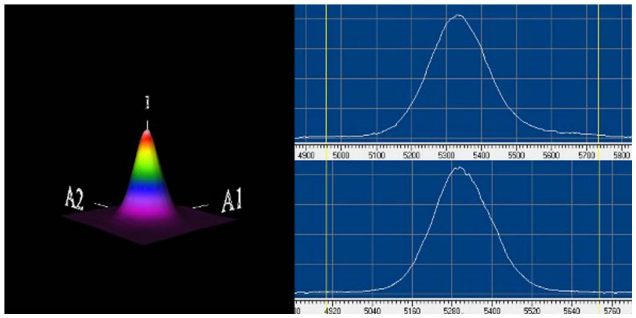

Fig. 8. Three-dimensional beam profile and power intensity distribution of 2.3 μm laser beam measured at the 1.84 W output power.

powers were, respectively, increased by 60%, 32%, 53%, and 75% compared with the 785 nm single-wavelength pumping. Due to the increased population in the $^3H_4$ level, the ESA process needs strong pumping to reach a high excitation rate in the $^3F_4 \rightarrow {}^3H_4$ two-level system.

The output beam profiles of dual-wavelength pumped 2.3 μm Tm:YLF lasers were monitored by a NanoScan beam analyzer (Photons Inc.). As shown in Fig. 8, the beam profiles of the 2308 nm beam were measured when the output powers of the 2308 nm laser with OC1 ($T = 1.5\%$) reached the maximum. By focusing the beam with a lens ($f = 100$ mm), the M^2 factors of the 2308 nm beam were measured to be 1.68 and 1.52 in the A1 and A2 directions, respectively. The polarization measurement showed that the 2.3 μm Tm:YLF laser was both π-polarized for 785 nm single-wavelength and dual-wavelength pumping.

4. Conclusion

In conclusion, we have used two wavelengths at 785 and 1470 nm to pump the 2.3 μm Tm:YLF laser, constructing the GSA and ESA dual-wavelength pumping scheme for the $^3H_4 \rightarrow {}^3H_5$ laser transition for the first time, to the best of our knowledge. Introducing an ESA pumping process can accurately excite the Tm^{3+} ions accumulated in the $^3F_4$ level to the $^3H_4$ level, enabling a double populating mechanism for the upper laser level $^3H_4$ of the 2.3 μm transition. When the second pump beam of 1470 nm was introduced, the oscillation threshold of the 2.3 μm laser was greatly reduced, and the output power was substantially increased. A maximum CW output power of 1.84 W at 2308 nm was achieved under 785 and 1470 nm dual-wavelength pumping, increased by 60% compared with the case of 785 nm single-wavelength pumping under the same resonator condition. Our work shows that the GSA ($^3H_6 \rightarrow {}^3H_4$) and ESA ($^3F_4 \rightarrow {}^3H_4$) dual-wavelength pumping scheme is an effective method to achieve higher-power 2.3 μm Tm laser output.

Acknowledgement

This work was supported by the National Natural Science Foundation of China (Nos. 61875077, 61911530131, and U1730119), the Natural Science Foundation of the Jiangsu Higher Education Institutions of China (No. 18KJA510001), and the Priority Academic Program Development of Jiangsu Higher Education Institutions (PAPD).

References

1. F. Canbaz, I. Yorulmaz, and A. Sennaroglu, "Kerr-lens mode-locked 2.3-μm Tm^{3+}:YLF laser as a source of femtosecond pulses in the mid-infrared," Opt. Lett. **42**, 3964 (2017).
2. I. Yorulmaz and A. Sennaroglu, "Low-threshold diode-pumped 2.3-μm Tm^{3+}:YLF lasers," IEEE J. Sel. Top. Quantum Electron. **24**, 1601007 (2018).
3. A. Muti, M. Tonelli, V. Petrov, and A. Sennaroglu, "Continuous-wave mid-infrared laser operation of Tm^{3+}:KY_3F_{10} at 2.3 μm," Opt. Lett. **44**, 3242 (2019).
4. A. Muti, F. Canbaz, M. Tonelli, J. E. Bae, F. Rotermund, V. Petrov, and A. Sennaroglu, "Graphene mode-locked operation of Tm^{3+}:$YLiF_4$ and Tm^{3+}:KY_3F_{10} lasers near 2.3 μm," Opt. Lett. **45**, 656 (2020).
5. A. Muti, I. Baylam, M. Tonelli, and A. Sennaroglu, "Tunable continuous-wave laser operation of Tm^{3+}:BaY_2F_8 near 2.3 μm," Opt. Lett. **45**, 4104 (2020).
6. J. Kwiatkowski, "Power and spectral analyses in diode-pumped *c*-cut Pbnm Tm:YAP laser," Chin. Opt. Lett. **18**, 091401 (2020).
7. C. Li, Y. X. Leng, and J. J. Huo, "$ReSe_2$ as a saturable absorber in a Tm-doped yttrium lithium fluoride (Tm:YLF) pulse laser," Chin. Opt. Lett. **17**, 011402 (2019).
8. H. T. Huang, S. Q. Wang, H. W. Chen, O. L. Antipov, S. S. Balabanov, and D. Y. Shen, "High power simultaneous dual-wavelength CW and passively-*Q*-switched laser operation of LD pumped Tm:YLF at 1.9 and 2.3 μm," Opt. Express **27**, 38593 (2019).
9. S. Q. Wang, H. T. Huang, H. W. Chen, X. Liu, S. D. Liu, J. L. Xu, and D. Y. Shen, "High efficiency nanosecond passively *Q*-switched 2.3 μm Tm:YLF laser using a $ReSe_2$-based saturable output coupler," OSA Continuum **2**, 1676 (2019).
10. E. Kifle, P. Loiko, L. Guillemot, J. L. Doualan, F. Starecki, A. Braud, T. Georges, J. Rouvillain, and P. Camy, "Watt-level diode-pumped thulium lasers around 2.3 μm," Appl. Opt. **59**, 7530 (2020).
11. A. Tyazhev, F. Starecki, S. Cozic, P. Loiko, L. Guillemot, A. Braud, F. Joulain, M. Tang, T. Godin, A. Hideur, and P. Camy, "Watt-level efficient 2.3 μm thulium fluoride fiber laser," Opt. Lett. **45**, 5788 (2020).
12. X. Chao, J. B. Jeffries, and R. K. Hanson, "Real-time, *in situ*, continuous monitoring of CO in a pulverized-coal-fired power plant with a 2.3 μm laser absorption sensor," Appl. Phys. B **110**, 359 (2013).
13. F. J. McAleavey, J. O'Gorman, J. F. Donegan, B. D. MacCraith, J. Hegarty, and G. Maze, "Narrow linewidth, tunable Tm^{3+}-doped fluoride fiber laser for optical-based hydrocarbon gas sensing," IEEE J. Sel. Top. Quantum Electron. **3**, 1103 (1997).
14. J. T. Olesberg, M. A. Arnold, C. Mermelstein, J. Schmitz, and J. Wagner, "Tunable laser diode system for noninvasive blood glucose measurements," Appl. Spectrosc. **59**, 1480 (2005).
15. S. T. Fard, W. Hofmann, P. T. Fard, G. Böhm, M. Ortsiefer, E. Kwok, M.-C. Amann, and L. Chrostowski, "Optical absorption glucose measurements using 2.3-μm vertical-cavity semiconductor lasers," IEEE Photon. Technol. Lett. **20**, 930 (2008).
16. J. Wagner, Ch. Mann, M. Rattunde, and G. Weimann, "Infrared semiconductor lasers for sensing and diagnostics," Appl. Phys. A **78**, 505 (2004).
17. Y. Morova, M. Tonelli, V. Petrov, and A. Sennaroglu, "Upconversion pumping of a 2.3 μm Tm^{3+}:KY_3F_{10} laser with a 1064 nm ytterbium fiber laser," Opt. Lett. **45**, 931 (2020).
18. L. Guillemot, P. Loiko, R. Soulard, A. Braud, J. L. Doualan, A. Hideur, R. Moncorgé, and P. Camy, "Thulium laser at ~2.3 μm based on upconversion pumping," Opt. Lett. **44**, 4071 (2019).
19. P. Loiko, R. Soulard, L. Guillemot, G. Brasse, J. L. Doulan, A. Braud, A. Tyazhev, A. Hideur, B. Guichardaz, F. Druon, and P. Camy, "Efficient

Tm:$LiYF_4$ lasers at ~2.3 μm: effect of energy-transfer upconversion," IEEE J. Quantum Electron. **55**, 1700212 (2019).
20. L. Guillemot, P. Loiko, R. Soulard, A. Braud, J. L. Doualan, A. Hideur, and P. Camy, "Close look on cubic Tm:KY_3F_{10} crystal for highly efficient lasing on the $^3H_4 \rightarrow {}^3H_5$ transition," Opt. Express **28**, 3451 (2020).
21. W. L. Gao, J. Ma, G. Q. Xie, J. Zhang, D. W. Luo, H. Yang, D. Y. Tang, J. Ma, P. Yuan, and L. J. Qian, "Highly efficient 2 μm Tm:YAG ceramic laser," Opt. Lett. **37**, 1076 (2012).
22. O. L. Antipov, A. A. Novikov, N. G. Zakharov, and A. P. Zinoviev, "Optical properties and efficient laser oscillation at 2066 nm of novel Tm:Lu_2O_3 ceramics," Opt. Mater. Express **2**, 183 (2012).
23. O. H. Sapir, J. Munch, and D. J. Ottaway, "Mid-infrared fiber lasers at and beyond 3.5 μm using dual-wavelength pumping," Opt. Lett. **39**, 493 (2014).
24. L. Guillemot, P. Loiko, A. Braud, J. Doualan, A. Hideur, M. Koselja, R. Moncorge, and P. Camy, "Continuouswave Tm:$YAlO_3$ laser at ~2.3 μm," Opt. Lett. **44**, 5077 (2019).